

# A Density Functional Study of Hyperfine Coupling Constants in Steroid Radicals

Philippe Lahorte,<sup>\*,†</sup> Frank De Proft,<sup>‡,||</sup> Freddy Callens,<sup>§,-</sup> Paul Geerlings,<sup>‡</sup> and Wim Mondelaers<sup>†</sup>

Department of Subatomic and Radiation Physics, Radiation Physics Group (Member of IBITECH), Gent University, Proeftuinstraat 86, B-9000 Gent, Belgium, Eenheid Algemene Chemie (ALGC), Free University of Brussels, Pleinlaan 2, B-1050 Brussels, Belgium, and Laboratory for Crystallography and Study of the Solid State, Gent University, Krijgslaan 281-S1, B-9000 Gent, Belgium

Received: July 20, 1999; In Final Form: October 13, 1999

We present the results of density functional calculations of <sup>1</sup>H hyperfine coupling constants (hfcc's) in four types of model steroid radicals (R1 through R4). The calculations are performed using the B3LYP functional in combination with Pople basis sets (6-31G(d) and 6-311G(d)) and the EPR-III basis set. In radicals R1, R2, and R3 the agreement between experimental and calculated isotropic hfcc's is excellent (differences < 5%) except for two protons in radical R3 where the calculations provide evidence for reconsidering the experimental assignment. The agreement is rather poor in the case of radical R4 and is indicative either of specific geometry effects that cannot be modeled in the proposed *isolated molecule* approach or of a different radical identity.

## Introduction

Over the past years, the formation of free radicals in a variety of steroid hormone crystals following high energy irradiation has been given considerable attention. This research is inspired both by the progress of radiation sterilization technology of pharmaceutical products and the investigation of radical intermediates in the metabolism of steroids.<sup>1</sup>

Steroid hormones are natural metabolites of cholesterol and differ from the latter by the presence of a coupled system of double bonds between the carbonyl group attached to the C3 atom and the carbon atoms C4 and C5. The androstane skeleton with the labeling of the rings and the carbon atoms is shown in Figure 1.

Radical products of steroid compounds created by high energy irradiation have also been thoroughly examined using electron paramagnetic resonance (EPR) and electron nuclear double resonance (ENDOR) spectroscopy.<sup>2,3</sup> As an overall result, it was found that the majority of radicals in  $\gamma$ -irradiated steroid hormones is created in the A and B rings. More specifically, four types of radicals have been identified or suggested.<sup>3</sup> They are displayed in Figure 2 and their structures will be discussed further on.

Complementary to these experimental techniques, theoretical quantum chemical calculations of hyperfine coupling constants (hfcc's) could be very valuable in the investigation of the identity and the electronic structure of the radicals involved. While a number of theoretical studies concerning geometries and electronic structure<sup>4</sup> and NMR chemical shifts<sup>5</sup> of steroids are already available, no thorough quantum chemical study of EPR

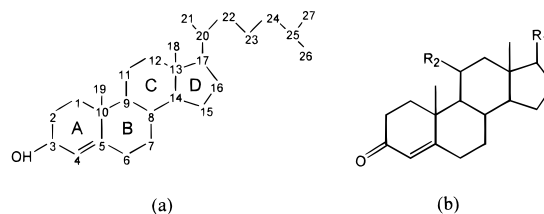


**Figure 1.** (a) Carbon atom labeling and ring notation for cholesterol; (b) the steroid skeleton [e.g., androgens (testosterone): R<sub>1</sub> = OH, R<sub>2</sub> = H].

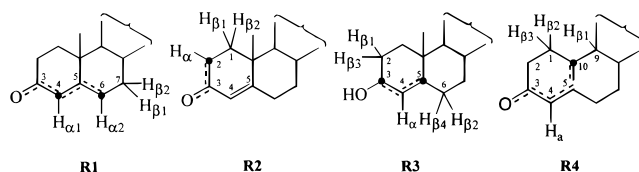


**Figure 2.** Schematic overview of the four types of radicals (labeled R1 through R4) formed in irradiated crystals of steroids.

spectroscopic properties has been performed yet. In the current study we present results on density functional theory (DFT) calculations of isotropic and anisotropic hyperfine coupling constants of <sup>1</sup>H atoms in various model steroid radicals. Comparisons are made with the available experimental data, and hypotheses are put forward with regard to the experimental assignment of coupling constants.

In recent years DFT has been of ever-increasing importance in the calculation of molecular ground state properties.<sup>6</sup> DFT has also emerged as the method of choice for the calculation of hyperfine coupling constants in small radicals mainly because of its cost-effective incorporation of electron interaction.<sup>7,8</sup> But DFT calculations have also been successfully applied for larger radical systems such as amino acids<sup>9</sup> and DNA radicals.<sup>10</sup> The aim of the present study is to further validate the usefulness and feasibility of DFT methods in the calculation of EPR spectroscopic properties of molecules that are of biological interest.

\* To whom correspondence should be addressed: fax, 32 (0)9 264 66 99; e-mail, Philippe.Lahorte@rug.ac.be

<sup>†</sup> Radiation Physics Group, Gent University.

<sup>‡</sup> Free University of Brussels.

<sup>§</sup> Laboratory for Crystallography and Study of the Solid State, Gent University.

<sup>||</sup> Postdoctoral Fellow of the Fund for Scientific Research–Flanders (Belgium) (F. W.O).

<sup>-</sup> Research Director of the Fund for Scientific Research–Flanders (Belgium) (F. W.O).

### Computational Details

For each of the radical species, a model system was constructed by neglecting the C and D rings from the steroid skeleton, as their influence on the hfcc's is expected to be small. Consequently, in each of the model radicals, the B ring was terminated with hydrogen atoms at the appropriate positions. The geometry optimization of these radicals was performed using the B3LYP functional<sup>11,12</sup> in combination with Pople's 6-31G(d) basis set,<sup>13</sup> starting from the available experimental crystal structure coordinates. No attempts were made to perform a full investigation of the geometric space for the respective radicals as this was beyond the scope of the present study that aims to represent suitable model systems for the compounds of interest. Subsequent single-point calculations were performed at the UB3LYP level using either Pople's standard 6-311 G(d) basis set or Barone's EPR-III set.<sup>8</sup> The latter is specifically tailored for the accurate calculation of EPR spectroscopic properties at the expense of a substantial extra computational burden. For the radical species under study, the 6-311G(d) set represents the optimal tradeoff between hfcc quality and computational burden for a series of Pople sets (6-31G(d), 6-31G(d,p), 6-311G(d), 6-311G(d,p), and 6-311G(2df,p)).<sup>14</sup> Frequency units (MHz) are used throughout this work when reporting values for hfcc's. All calculations were accomplished using the *Gaussian 98* software.<sup>15</sup>

The formulas for calculating experimental hyperfine parameters, assuming an isotropic  $g$ -tensor,  $S = 1/2$ , and  $I = 1/2$ , are obtained from the spin Hamiltonian

$$H = g \beta_e S_z B - g_N \beta_N I_z B + S A I$$

The first two contributions are the electronic and the nuclear Zeeman terms, respectively, caused by the interaction of the magnetic field  $B$  that defines the  $z$ -direction and the magnetic moments of the electrons or nuclei in the system;  $g$  and  $g_N$  are the electron and nuclear magnetogyric ratios, and  $\beta_e$ ,  $\beta_N$  the Bohr and nuclear magnetons. The remaining term is the hyperfine interaction term and results from the interaction between the unpaired electrons and the nucleus ( $I \neq 0$ ).

The  $3 \times 3$  hyperfine interaction matrix  $A$  can be separated into an isotropic, spherically symmetric part (Fermi interaction) and dipolar, anisotropic components. The isotropic hyperfine splittings  $A_{\text{iso}}$  are related to the spin densities at the positions of the corresponding nuclei by

$$A_{\text{iso}} = \frac{2}{3} \mu_0 g \beta_e g_N \beta_N |\psi(0)|^2$$

In this expression,  $\mu_0$  is the magnetic permeability in a vacuum and  $|\psi(0)|^2$  the probability of finding the electron at the nucleus. From the classical expression of interacting dipoles at a distance  $r$ , the anisotropic components  $A_{\alpha\beta}$  ( $\alpha, \beta = x, y, z$ ) are derived as

$$A_{\alpha\alpha} = \frac{\mu_0}{4\pi} g \beta_e g_N \beta_N \left\langle \frac{3\alpha^2 - r^2}{r^5} \right\rangle$$

$$A_{\alpha\beta} = \frac{\mu_0}{4\pi} g \beta_e g_N \beta_N \left\langle \frac{3\alpha\beta}{r^5} \right\rangle$$

with the angular brackets indicating spatial integration over the electron wave function.

### Results and Discussion

**Radical R1.** Abstraction of a proton from the carbon atom C6 results in the model radical R1 depicted in Figure 3. The

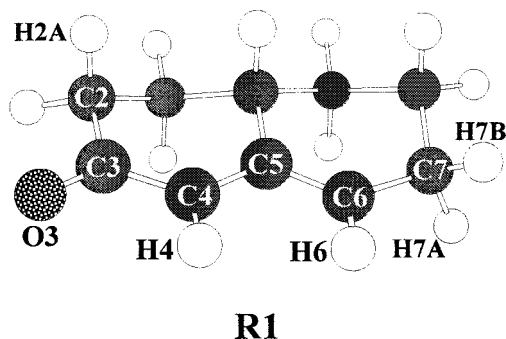


**Figure 3.** The model radical R1.

UB3LYP/6-311G(d)//B3LYP/6-31G(d) spin densities are 0.21 at O3 (0.20 with EPR-III) and 0.55 both at C4 and C6 (0.52 with EPR-III), effectively leading to an  $\alpha$  coupling at the atoms H4 and H6 and two  $\beta$  couplings at H7A and H7B. Previously, spin densities for C4 and C6 of 0.44 and 0.45, respectively, were estimated from experimental data.<sup>16</sup>

The calculated hfcc's for the hydrogen atoms H4 and H6 compare excellently with the experimental values, as can be seen from Table 1. Experimentally, the H6 isotropic hfcc is slightly more negative (0.6–0.8 MHz) than the corresponding value of H4. This is reproduced by the calculations that point toward a difference of about 1 MHz.

The angles of H7A and H7B with the radical plane formed by C7–C6–C5 are  $-110.1^\circ$  and  $136.0^\circ$ , respectively. When analyzing the multitude of experimental data available for the H7A and H7B couplings, it becomes clear that geometry effects, due to different crystal lattice parameters of the various steroid molecules, result in subtle changes in the measured hfcc's. However the calculated isotropic hfcc's (averaged over the 6-311G(d) and the EPR-III calculation) deviate less than 5% of the average corresponding experimental values.

Additionally, Henriksen and Sagstuen reported a small coupling with an isotropic value of 7.2 MHz and tentatively assigned it to the  $\gamma$  proton H2A.<sup>17</sup> Whereas, experimentally, the angle formed by the unpaired electron orbital and the H2–C2–C3 plane is  $3.3^\circ$  for H2A and  $54.5^\circ$  for H2B,<sup>19</sup> the corresponding values at the B3LYP/6-31G(d) level in our model radical are  $6.5^\circ$  and  $49.0^\circ$ . For the correct modeling of the geometry effects responsible for small discrepancies as in the case of the atom H2A, the influence of nearest neighboring atoms in the crystal lattice will have to be incorporated in the geometry optimization procedure. However, this issue is beyond the scope of the present study and adds little new information to the identification of the radical R1.

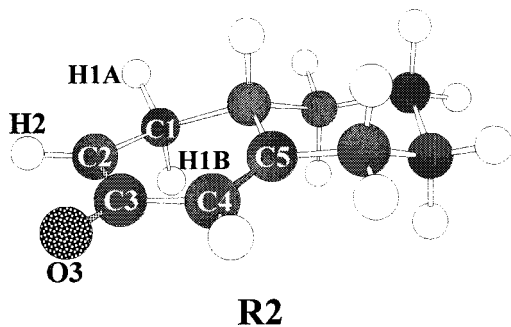
**Radical R2.** The radical R2, as shown in Figure 4, is formed by abstraction of a hydrogen atom from C2. The unpaired spin density is distributed over the atoms C2 and O3 as reflected by the respective atomic spin densities of 0.83 and 0.28 (0.80 and 0.30 with EPR-III). A value of 0.7 for C2 was previously calculated from experimental data.<sup>18</sup> This results both in an  $\alpha$  coupling at the hydrogen H2 and two  $\beta$  couplings for H1A and H1B. The dihedral angles of H1A and H1B, with respect to the fragment C1–C2–C3, are  $89.9^\circ$  and  $-55.9^\circ$ , respectively. All calculated values, presented in Table 2, differ less than 5.5% from the reported experimental couplings.

**Radical R3.** Addition of a hydrogen atom at the oxygen atom O3 produces the radical R3 (see Figure 5). The methyl group at the C10 position was included in the model as two of its hydrogen atoms provide steric hindrance for the axial hydrogens H2A at the C2 position and H6A at the C6 position. This results in dihedral angles H2A–C2–C3–C4 and H6A–C6–C5–C4

**TABLE 1: Experimental and Calculated hfcc's (MHz) for the Model Steroid Radical R1**

molecule, method, [reference]	H4		H6		H7A		H7B		H2A	
	$A_{\text{iso}}$	$A_{\text{xx}}$ $A_{\text{yy}}$ $A_{\text{zz}}$	$A_{\text{iso}}$	$A_{\text{xx}}$ $A_{\text{yy}}$ $A_{\text{zz}}$	$A_{\text{iso}}$	$A_{\text{xx}}$ $A_{\text{yy}}$ $A_{\text{zz}}$	$A_{\text{iso}}$	$A_{\text{xx}}$ $A_{\text{yy}}$ $A_{\text{zz}}$	$A_{\text{iso}}$	$A_{\text{xx}}$ $A_{\text{yy}}$ $A_{\text{zz}}$
Experimental										
cholest-4-en-3-one, EPR, [21] <sup>a,b</sup>	-32.8	-49.3 -31.7 -17.4			50.2		73.8			
cholesta-4,6-diene-3-one, EPR, [22] <sup>a</sup>	-31.4	-47.1 -29.1 -17.9			54.9		73.1			
progesterone, EPR, [23] <sup>a,b</sup>	-33.1	-46.0 -28.6 -24.9	-	-	51.1	55.5 49.3 48.5	71.4	74.5 70.9 68.7		
17- $\alpha$ -hydroxy-progesterone, EPR, [24] <sup>a</sup>	-30.8	-50.2 -28.0 -14.3			55.2	57.4 55.2 53.0	72.3	79.0 72.3 65.6		
androst-4-en-3,17-dione, EPR, [25] <sup>a</sup>	-33.1	-48.8 -33.3 -17.1			49.6	54.4 49.6 45.1	72.6	76.6 72.0 69.8		
cholest-4-en-3-one, ENDOR, [16]	-31.7	-46.3 -33.5 -15.4	-32.3	-48.0 -33.3 -15.4	50.5	55.3 48.6 47.6	73.4	78.3 71.6 70.4		
progesterone, ENDOR, [17]	-31.1	-45.4 -33.0 -15.0	-31.9	-47.5 -33.0 -15.3	50.2	54.9 48.2 47.5	71.9	76.8 70.0 68.8	10.5 7.2 6.9	4.3 4.3
Calculated [This Work]										
UB3LYP/6-311G(d)	-31.8	-47.2 -35.9 -12.3	-32.8	-49.7 -36.4 -12.2	44.3	49.3 42.2 41.3	71.2	76.4 69.3 67.9	-1.7	0.9 -2.7 -3.4
UB3LYP/EPR-III	-32.6	-48.4 -35.0 -14.4	-33.7	-51.2 -35.3 -14.6	48.2	53.4 46.1 45.1	77.5	83.0 75.4 74.1	-0.9	1.7 -1.9 -2.6

<sup>a</sup> Experimentally, the sign of the  $\alpha$  coupling (H4 and H6) was not determined. <sup>b</sup> Although the ENDOR data in this table for these molecular systems are more accurate, the EPR data are retained for the sake of comprehensiveness.

**Figure 4.** The model radical R2.

of  $-99.5^\circ$  and  $-99.9^\circ$ , respectively. The corresponding experimental, undamaged crystal values in cholest-4-en-3-one are  $-94.5^\circ$  and  $-105.2^\circ$ .<sup>20</sup> When comparing these angles, however, one has to take into account that some molecular rearrangement takes place upon formation of the radical.

The unpaired electron is distributed over the atoms C3 and C5 with atomic spin densities of 0.49 and 0.64, respectively. A negative spin density of  $-0.22$  is localized at C4, resulting in an allyl-type coupling at proton H4, which is very well reproduced. From the experimental coupling constants, the respective C3, C5, and C4 spin densities were estimated to be 0.43, 0.41, and  $-0.11$ .<sup>16</sup>

The agreement between experiment and calculations is also very good for the two equatorial  $\beta$  type couplings at protons H2B and H6B. There is, however, a poor correspondence for the two axial  $\beta$  type couplings (protons H2A and H6A). Therefore, the experimental assignment of the two involved couplings was reinvestigated. An important argument in this

**TABLE 2: Experimental<sup>18</sup> and Calculated hfcc's (MHz) for the Model Steroid Radical R2**

molecule, method, [reference]	H2		H1A		H1B	
	$A_{\text{iso}}$	$A_{\text{xx}}$ $A_{\text{yy}}$ $A_{\text{zz}}$	$A_{\text{iso}}$	$A_{\text{xx}}$ $A_{\text{yy}}$ $A_{\text{zz}}$	$A_{\text{iso}}$	$A_{\text{xx}}$ $A_{\text{yy}}$ $A_{\text{zz}}$
Experimental						
testosterone (monocline), EPR, [18] <sup>a</sup>	-51.8	-79.3 -51.3 -25.5	37.3		135.6	
Calculated [This Work]						
UB3LYP/6-311G(d)	-49.6	-77.8 -53.8 -17.1	36.2	43.6 32.7 32.2	128.5	136.3 126.0 120.3
UB3LYP/EPR-III	-51.0	-79.7 -52.2 -21.0	40.5	48.0 37.1 36.4	142.6	150.7 139.6 137.5

<sup>a</sup> Experimentally, the sign of the  $\alpha$  coupling (H2) was not determined.

respect comes from the analysis of the eigenvectors associated with the anisotropic hfcc's. For  $\beta$  protons with small dihedral angles with respect to the unpaired electron orbital, the direction of the maximum coupling is expected to occur close to the direction of the corresponding  $C_\beta-H_\beta$  bond. Consequently, comparison of these directions is helpful in the experimental assignment of couplings. This was basically also the approach followed by Andersen et al., completed with calculations at the INDO RHF + CI level.<sup>16</sup> However, of crucial importance in this particular case is the fact that, experimentally, the C2-H2A and C6-H6A bond directions are nearly coincident in the crystal lattice, prohibiting any conclusive assignment of the observed couplings.

TABLE 3: Experimental<sup>16</sup> and Calculated hfcc's (MHZ) for the Model Steroid Radical R3

molecule, method, [reference]	H4		H2A		H6A		H2B		H6B	
	A <sub>iso</sub>	A <sub>xx</sub> A <sub>yy</sub> A <sub>zz</sub>								
Experimental										
cholest-4-en-3-one, ENDOR, [16]	8.0	12.3 8.5 3.3	72.5	77.9 70.1 69.5	69.5	65.4 58.6 57.7	24.3	29.2 22.3 21.4	7.4	12.8 5.2 4.4
Calculated [This Work]										
UB3LYP/6-311G(d)	8.1	13.6 7.2 3.5	55.7	60.7 53.7 52.7	71.2	77.0 68.6 68.0	20.4	25.4 18.4 17.4	7.0	12.6 4.6 3.8
UB3LYP/EPR-III	10.0	15.8 9.4 4.8	61.7	67.0 59.6 58.5	77.0	83.0 74.2 73.8	23.2	28.3 21.2 20.0	7.7	13.3 5.3 4.5

TABLE 4: Experimental<sup>16</sup> and Calculated hfcc's (MHZ) for the Model Steroid Radical R4

molecule, method, [reference]	H4		H9		H1A		H1B		A1		A2	
	A <sub>iso</sub>	A <sub>xx</sub> A <sub>yy</sub> A <sub>zz</sub>										
Experimental												
cholest-4-en-3-one, ENDOR, [16]	-24.9	-35.5 -25.7 -13.4	52.1	55.9 50.6 49.8	37.9	41.6 36.4 35.7	12.7	16.0 11.4 10.8	5.1	11.0 7.6 -3.4	5.2	8.1 4.2 3.4
Calculated [This Work]												
UB3LYP/6-311G(d) <sup>a</sup>	-34.6	-53.6 -37.1 -13.0	65.1	70.1 63.0 62.1	58.2	62.8 56.8 55.1	11.9	16.5 10.0 9.2				
UB3LYP/6-311G(d) <sup>b</sup>	-24.5	-40.0 -26.7 -6.8	72.5	77.1 71.2 70.2	61.2	66.3 59.8 57.5	13.5	19.9 10.4 10.2				

<sup>a</sup> B3LYP/6-31G(d) level of optimization of all internal coordinates in the model radical of Figure 6. <sup>b</sup> The distance of C10 to the C1-C5-C9 plane in the radical of Figure 6 is fixed to 0.35 Å; geometry reoptimization of all other internal coordinates at the B3LYP/6-31G(d) level.

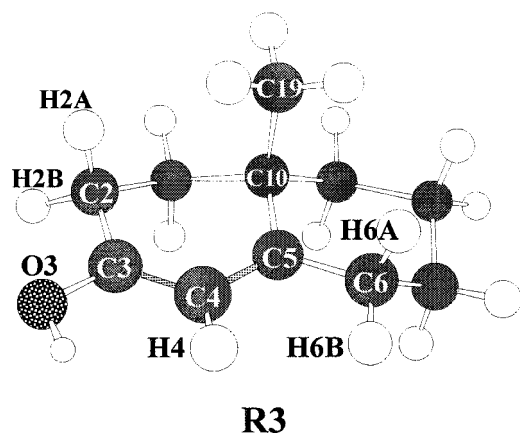


Figure 5. The model radical R3.

Therefore, also taking into account the high quality of the calculations as demonstrated in the cases of radicals R1 and R2, we suggest that the value of 72.5 MHz, experimentally assigned to the H2A atom, in fact corresponds to the UB3LYP/6-311G(d) calculated value of 71.2 MHz of atom H6A and vice versa for the experimental and calculated values of H6A and H2A, respectively. In our view, this particular case presents an example of the potential of this type of calculations toward elucidation of experimental spectra.

**Radical R4.** The radical R4 is formed by scission of the C10-C19 bond (see Figure 6). Calculated spin densities are 0.54, 0.57, and 0.20 at the C10, C4, and O3 atoms, respectively (0.52, 0.50, and 0.20 with EPR-III). The respective C10 and

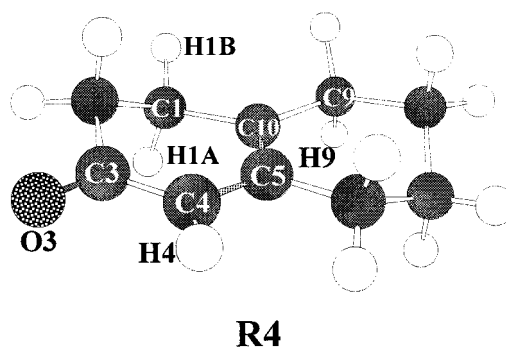
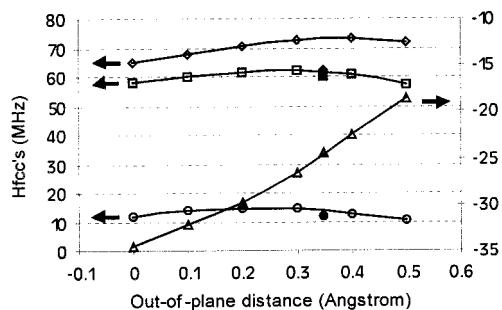


Figure 6. The model radical R4.

C4 values, calculated from the experimental hfcc's, are 0.33 and 0.35.<sup>16</sup>

As can be seen from Table 4, the correspondence between experimental and calculated hfcc's is poor for all atoms, with the exception of the  $\beta$ -type coupling at atom H1B, which is in the equatorial position. A combination of factors might be responsible for the noted discrepancies. First of all, of the four types of model radicals under study, the changes in the molecular conformation upon creation of the radical are likely to be the largest in the radical R4 as its formation consists of a transition from a tetrahedral to a planar structure for the central atom C10 which is connecting the A and B rings. In contrast, the conformational changes involved in the formation of radicals R1 and R2 are in essence restricted to a change in hybridization state of only one ring atom (C6 and C2, respectively) and in radical R3, the hybridization state of the ring atoms is not altered at all. Also, the fact of omitting the C ring from the model



**Figure 7.** Proton hfcc's upon variation of the distance of the atom C10 to the C1–C5–C9 plane (reoptimization of all other internal coordinates). (A) in the limited model radical of Figure 6: ( $\Delta$ ) H4, ( $\square$ ) H1A, ( $\circ$ ) H1B, ( $\diamond$ ) H9; (B) in the extended model radical of Figure 8: ( $\blacktriangle$ ) H4, ( $\blacksquare$ ) H1A, ( $\bullet$ ) H1B, ( $\blacklozenge$ ) H9. All values are in MHz; UB3LYP/6-311G(d)//B3LYP/6-31G(d) level of calculation.

radical structure could have larger consequences for R4 than for the other types of radicals as the equilibrium position of the protons responsible for the couplings will be more affected in the former (e.g., H9 in R4). Some of these effects were further investigated.

At the B3LYP/6-31G(d) optimized geometry, the carbon atom C10 has perfect  $sp^2$  character and is located in the C1–C5–C9 radical plane, thus effectively maximizing the delocalization of the unpaired spin density over the C10–C4–O3 system. The calculated C4 spin density results in an H4 hfcc that drastically overshoots the experimental value. This discrepancy could be explained by the fact that in reality the unpaired spin density delocalization is less pronounced due to a partial  $sp^3$  character of the C10 atom. Indeed, the split-off  $^{\text{C}}\text{CH}_3$  radical, whose exact position in the crystal lattice is unknown, might have this effect on the C10 atom. To investigate this issue, the C10 atom was lifted up to 0.5 Å above the C1–C5–C9 plane in steps of 0.1 Å, thus effectively mimicking an increasing  $sp^3$  character. While keeping fixed the resulting angles C1–C10–C5, C5–C10–C9, and C9–C10–C1, reoptimization of all other internal coordinates of the radical was performed at the B3LYP/6-31G(d) level. The resulting hfcc's of the relevant protons are displayed in Figure 7. A distance of C10 to the C1–C5–C9 plane of about 0.35 Å leads to the best fit between experimental and calculated values for the  $\alpha$  coupling of proton H4 and the  $\beta$  coupling of the proton H1B that is in an equatorial position. The corresponding hfcc's are displayed in Table 4. Over the whole range of calculated distances there is no agreement for the axially located H1A and H9 proton hfcc's. To determine whether this effect could arise from the limited size of the model radical, exactly the same type of calculations were performed on the *extended* model radical displayed in Figure 8, for a distance of 0.35 Å. This model radical is closer to the true steroid structure by incorporation of the C-ring. As discussed above, this might result in significant changes in the H1A and H9 isotropic hfcc's through changes of the equilibrium geometry. The H9–C9–C10–C5 and H1A–C1–C10–C5 dihedral angles change from 85.9° and –74.5° in the limited model of Figure 6 to 82.2° and –69.7° in the extended model, respectively. Only the H9 isotropic hfcc decreases by about 10 MHz while the other reported couplings change very little (see Figure 7). Thus, extending the model steroid structure by including the C ring does not result in a substantial improvement of the agreement with the experimental hfcc's.

Experimentally, two additional small couplings, A1 and A2, were reported by Andersen et al.,<sup>16</sup> who suggested they might be due to  $\beta$ ,  $\gamma$ , or even  $\gamma$  protons. No attempt was made in the current study to assign these couplings.

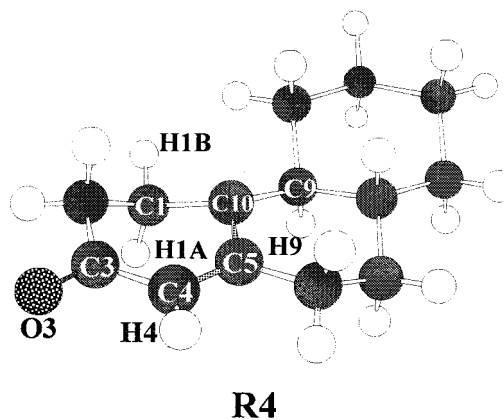


**Figure 8.** The extended model radical R4.

In conclusion, the *isolated molecule* approach is only partially successful in the case of the radical R4. In our opinion, the excellent quality of the calculations, as demonstrated in the case of the radicals R1, R2, and R3, presents an indication of the involvement of subtle geometry effects. To resolve this issue, a more complex simulation, explicitly involving nearest neighboring atoms in the crystal lattice, should be performed. The feasibility of this issue is currently under investigation.

On the other hand, as no indications are available that the modeling of subtle geometry effects is appropriate in the radicals R1 through R3, the possibility should be kept open that the proposed model structure for R4 is incorrect. In this case, a different radical identity has to be proposed in concordance with the experimental observations.

## Conclusions

We have presented density functional theory calculations of isotropic and anisotropic hyperfine coupling constants of model steroid radicals. Overall, a very good agreement between calculated and experimental values is obtained (differences < 5%) and the majority of the reported experimental assignments are confirmed. In the case of the radical R3 the calculations provide evidence for reconsidering the experimental assignment for the protons H2A and H6A. The poor agreement in the case of radical R4 is indicative either of specific geometry effects that cannot be modeled in the proposed *isolated molecule* approach or of a different radical identity.

The use of the higher calculational quality EPR-III basis set for single point hfcc calculations in combination with the B3LYP functional outweighs the substantial extra computational burden only in those few cases where very subtle geometry effects can hamper the conclusive assignment of couplings (e.g., protons H2A and H6A in radical R3). In all other cases, the Pople 6-311G(d) basis set performs adequately.

The results of this study present an example of the feasibility of high-level, standard DFT calculations of hyperfine couplings in biologically relevant radicals and demonstrate both the power and limitations of these quantum chemical methods toward elucidation of experimental EPR spectra.

**Acknowledgment.** This work has been performed in the framework of a Concerted Research Action (GOA-12050695) with financial support from the Research Board of the University Gent. F. De Proft, F. Callens, and W. Mondelaers greatly acknowledge the F.W.O. Flanders (Belgium).

**Supporting Information Available:** Optimized geometries in Cartesian coordinates for radicals R1 through R4. This

material is available free of charge via the Internet at <http://pubs.acs.org>.

## References and Notes

- (1) Moriarity, N. J.; Maerker, G. *J. Am. Oil Chem. Soc.* **1990**, *67*, 923. Maerker, G.; Jones, K. C. *J. Am. Oil Chem. Soc.* **1992**, *69*, 451. Maerker, G.; Jones, K. C. *J. Am. Oil Chem. Soc.* **1993**, *70*, 255.
- (2) Szyzewski, A.; Endeward, B.; Möbius, K. *Appl. Radiat. Isot.* **1998**, *49*, 59.
- (3) Szyzewski, A. *Appl. Radiat. Isot.* **1996**, *47*, 1675, and references therein.
- (4) Kubli-Garfias, C. *J. Mol. Struct. (THEOCHEM)* **1998**, *422*, 167. Kubli-Garfias, C. *J. Mol. Struct. (THEOCHEM)* **1998**, *425*, 171; Pasatolic, L. J.; Klasinc, L.; Spiegl, H.; Knop, J. V.; McGlynn, S. P. *Int. J. Quantum Chem.* **1992**, *41*, 815.
- (5) Smith, W. B. *Magn. Reson. Chem.* **1999**, *37*, 103.
- (6) Geerlings, P.; De Proft, F.; Langenaeker, W. *Adv. Quantum Chem.* **1999**, *33*, 303.
- (7) Malkin, V. G.; Malkina, O. L.; Eriksson, L. A.; Salahub, D. R. In *Modern Density Functional Theory: A Tool for Chemistry*; Pulitzer, P., Seminario, J. M., Eds.; Elsevier: Amsterdam, 1995; Chapter 9.
- (8) Barone, V. In *Recent Advances in Density Functional Methods*, Part I; Chong, D. P., Ed.; World Scientific Publishing Co.: Singapore, 1995; Chapter 8.
- (9) Lahorte, P.; De Proft, F.; Vanhaelewyn, G.; Masschaele, B.; Cauwels, P.; Callens, F.; Geerlings, P.; Mondelaers, W. *J. Phys. Chem. A* **1999**, *103*, 6650. Ban, F.; Wetmore, S.; Boyd, R. *J. Phys. Chem. A* **1999**, *103*, 4303.
- (10) Wetmore, S. D.; Boyd, R. J.; Eriksson, L. A. *J. Phys. Chem. B* **1998**, *102*, 10602. Wetmore, S. D.; Boyd, R. J.; Eriksson, L. A. *J. Phys. Chem. B* **1998**, *102*, 9332. Wetmore, S. D.; Boyd, R. J.; Eriksson, L. A. *J. Phys. Chem. B* **1998**, *102*, 7674. Wetmore, S. D.; Boyd, R. J.; Eriksson, L. A. *J. Phys. Chem. B* **1998**, *102*, 5369.
- (11) Becke, A. D. *J. Chem. Phys.* **1993**, *98*, 5648.
- (12) Lee, C.; Yang, W.; Parr, R. G. *Phys. Rev B* **1988**, *37*, 785. Stevens, P. J.; Devlin, F. J.; Chablowski, C. F.; Frisch, M. J. *J. Phys. Chem.* **1994**, *98*, 11623.
- (13) Pople, J.; Beveridge, D.; Dobosh, P. *J. Am. Chem. Soc.* **1968**, *90*, 4201.
- (14) This work, data is available from the authors upon request.
- (15) *Gaussian 98*, Revision A.6. Frisch, M. J.; Trucks, G. W.; Schlegel, H. B.; Scuseria, G. E.; Robb, M. A.; Cheeseman, J. R.; Zakrzewski, V. G.; Montgomery, J. A., Jr.; Stratmann, R. E.; Burant, J. C.; Dapprich, S.; Millam, J. M.; Daniels, A. D.; Kudin, K. N.; Strain, M. C.; Farkas, O.; Tomasi, J.; Barone, V.; Cossi, M.; Cammi, R.; Mennucci, B.; Pomelli, C.; Adamo, C.; Clifford, S.; Ochterski, J.; Petersson, J. A.; Ayala, P. Y.; Cui, Q.; Morokuma, K.; Malick, D. K.; Rabuck, A. D.; Raghavachari, K.; Foresman, J. B.; Cioslowski, J.; Ortiz, J. V.; Stefanov, B. B.; Liu, G.; Liashenko, A.; Piskorz, P.; Komaromi, I.; Gomperts, R.; Martin, R. L.; Fox, D. J.; Keith, T.; Al-Laham, M. A.; Peng, C. Y.; Nanayakkara, A.; Gonzalez, C.; Challacombe, M.; Gill, P. M. W.; Johnson, B.; Chen, W.; Wong, M. W.; Andres, J. L.; Gonzalez, C.; Head-Gordon, M.; Replogle, E. S.; Pople, J. A.; Gaussian, Inc.: Pittsburgh, PA, 1998.
- (16) Andersen, M. F.; Sagstuen, E.; Henriksen, T. *J. Magn. Reson.* **1987**, *71*, 461.
- (17) Henriksen, T.; Sagstuen, E. *J. Magn. Reson.* **1985**, *63*, 333.
- (18) Szyzewski, A.; Krzyminiewski, R.; Hafez, A. M.; Pietrzak, J. *Int. J. Radiat. Biol.* **1986**, *50*, 841.
- (19) Campsteyn, H.; Dupont, L.; Dideberg, O. *Acta Crystallogr. B* **1972**, *28*, 3032.
- (20) Sheldrick, G. M.; Oeser, E.; Caira, M. R.; Nassimbene, L. R.; Pauptit, R. A. *Acta Crystallogr. B* **1976**, *32*, 1984.
- (21) Krzyminiewski, R.; Hafez, A. M.; Pietrzak, J.; Szyzewski, A. *J. Magn. Reson.* **1983**, *51*, 308.
- (22) Hafez, A. M.; Krzyminiewski, R.; Szyzewski, A.; Pietrzak, J. *J. Mol. Struct.* **1985**, *130*, 301.
- (23) Krzyminiewski, R.; Masiakowski, J.; Pietrzak, J.; Szyzewski, A. *J. Magn. Reson.* **1982**, *46*, 300.
- (24) Krzyminiewski, R.; Pietrzak, J.; Konopka, R. *J. Mol. Struct.* **1990**, *240*, 133.
- (25) Krzyminiewski, R.; Hafez, A. M.; Szyzewski, A.; Pietrzak, J. *J. Mol. Struct.* **1987**, *160*, 127.